Chromium Raises Vacancy Concentration and Promotes Grain-Boundary Al Segregation in Ni–Cr–Al

Stephen T.W. Kerr[a], Keyvan Ferasat[a,b], Yasaman Ghaffari[b], Kevin Daub[a], Suraj Y. Persaud[a], Laurent Karim Béland[a,*]

[a] *Department of Mechanical and Materials Engineering, Queen's University, Kingston, Ontario, Canada*
[b] *Canadian Nuclear Safety Commission, Ottawa, Ontario, Canada*

Abstract

Chromium additions are known to promote the formation of a protective Al oxide, alumina, in Ni-Cr-Al alloys, a phenomenon known as the third-element effect (TEE). Using atomistic simulations, we show that Cr lowers vacancy formation energies while leaving migration barriers largely unchanged. This reduction in formation energy leads to a strong amplification of equilibrium vacancy concentrations: compared to Ni–4Al, the concentration in Ni–15Cr–4Al is 11 times higher at 1000 °C and more than 54 times higher at 480 °C. When combined with tracer mobilities, this produces effective diffusion coefficients up to an order of magnitude greater in the ternary alloy. In parallel, Cr promotes aluminum enrichment at grain boundaries, raising Al levels to about one and a half times the bulk concentration across the boundaries studied. These metal-phase mechanisms provide a quantitative route by which Cr facilitates rapid Al delivery to oxidation fronts, complementing oxygen-gettering models and helping explain the TEE, at both high and intermediate homologous temperatures.

Keywords: Ni-Cr-Al, third-element effect, vacancy formation energy, grain boundary segregation, diffusion, NEB, LAMMPS

1

Many industrial alloys derive their oxidation resistance from high chromium (Cr) and aluminum (Al) content, which enables the formation of a stable, protective alumina film that inhibits further oxidation[1–7]. By contrast, Ni–Al alloys with insufficient Al form non-protective NiO scales at elevated temperatures, leading to internal oxidation. The addition of Cr promotes the selective formation of alumina, a phenomenon known as the third-element effect (TEE), which has also been reported in other alloy systems, including Fe–Cr–Al and Cu–Zn–Ni[8].

Using atomistic simulations, we find that raising the Cr at% lowers vacancy formation energies while leaving migration barriers largely unchanged. At equilibrium, the vacancy fraction follows $c_v \propto \exp[-E_f/(k_B T)]$. A 0.28 eV reduction in E_f from Ni–4Al to Ni–15Cr–4Al yields vacancy concentrations 11 times higher at 1000 °C and more than 54 times higher at 480 °C . When combined with tracer mobilities, this produces effective diffusion coefficients up to an order of magnitude greater in the ternary alloy. Cr also enhances Al enrichment at grain boundaries, raising Al levels to about 1.5 times the bulk concentration across the Σ3/5/11 boundaries studied. These metal-phase mechanisms provide a quantitative route by which Cr accelerates Al delivery to oxidation fronts, complementing oxygen-getter models of the TEE.

The classical hypothesis, proposed by Wagner[8], posits that Cr acts as a secondary oxygen getter. By temporarily sequestering oxygen at the alloy surface, Cr reduces inward oxygen diffusion, providing additional time for Al to diffuse and form a thermodynamically stable Al_2O_3 layer. According to Wagner's model, this behaviour emerges once a critical combined concentration of Cr and Al is exceeded.

At intermediate homologous temperatures (∼500 °C for Ni-based alloys), where bulk diffusion is negligible but short-circuit transport along GBs remains active, oxidation proceeds primarily via GB pathways. In binary systems, Ghaffari *et al.*[9] showed that Ni–(11,15)Cr alloys tend to form Cr-rich scales, while Ni–(4,7)Al alloys display similar oxidation independent Al content: Ni–Al alloys develop narrow, oxides penetrating inward along GBs. Extending this work to ternaries, Ghaffari *et al.*[10] demonstrated that adding significant Cr to low Al Ni-Al alters its oxidation response to resemble that of Ni–Al rather than Ni–Cr. Cr additions promoted Al segregation to GBs, enabling localized Al-rich oxide formation. Microstructurally, high-angle GBs developed dual-layer surface oxides containing both Al- and Cr-rich phases, while low-angle and coincidence-site lattice boundaries exhibited porous intergranular Al-rich oxides encased by Cr-rich shells[10]. Together, these studies show both the GB-character dependence of oxidation and the role of Cr in amplifying Al's scale-forming effectiveness at such intermediate temperatures. In other words, they describe an intermediate-temperature manifestation of the

*Corresponding author.
Email addresses: laurent.beland@queensu.ca (Laurent Karim Béland), laurent.beland@queensu.ca (Laurent Karim Béland)

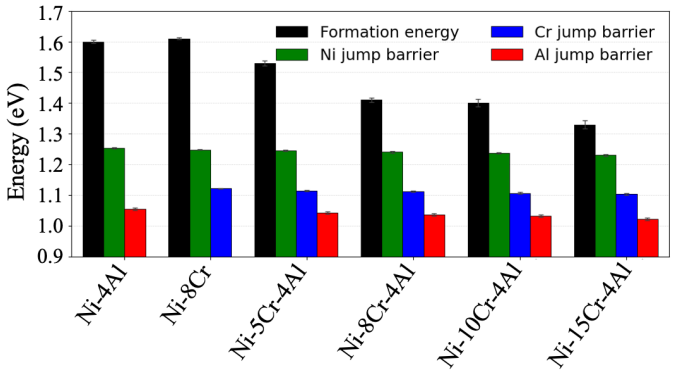

Figure 1: Vacancy formation energies and average vacancy jump barriers. Formation energies decrease with increasing Cr content, while NEB-derived migration barriers do not. Vacancy jumps to Al lattice sites have the lowest barriers, followed by Cr and Ni. NEB barriers were averaged over 1,000 randomly perturbed jump pathways per species. Error bars represent standard errors.

TEE.

In parallel with these experimental developments, computational studies have focused on point defect transport in oxide phases. For example, Ullberg *et al.*[11] showed that vacancies form more readily than interstitials in Cr_2O_3 and that Mn substitution can enhance vacancy-mediated diffusion. Banerjee *et al.*[12] demonstrated that vacancy transport underpins mass transfer in Fe_2O_3, while Xiao *et al.*[13] explored oxidation in Ni–Cr alloys, identifying metal/vacancy fluxes in the sub-oxide region as key to determining which oxide type will form (NiO spinels versus Cr_2O_3).

Diffusion of point defects in the metallic phase of alloys (i.e. before oxidation) has also been widely studied, including recent simulations addressing binary and ternary systems[14–31]. However, these studies have not directly linked point defect diffusion to the TEE, nor have they considered the role of different GB types in controlling elemental segregation relevant to oxidation resistance.

Here, we address these gaps by using atomistic simulations to probe how the addition of Cr influences vacancy-mediated diffusion and grain-boundary segregation in Ni–Al alloys. We show how Cr alters vacancy formation energies and mobilities in the bulk, and how it modifies Al segregation across different GB types, thereby clarifying the mechanisms by which Cr enables the experimentally observed TEE.

In this short communication, we first present results on vacancy energetics, and then results on grain-boundary segregation. We discuss their implications for the third-element effect.

We employed atomistic simulations to examine how varying Cr concentration affects chemical potentials, vacancy formation and migration energies, diffusion coefficients, and grain-boundary (GB) segregation in Ni–Cr–Al alloys. All simulations were performed using the Large-scale Atomic/Molecular Massively Parallel Simulator (LAMMPS) [32], with the embedded atom method (EAM) potential of Farkas *et al.* [33]. This potential was parameterized to reproduce heats of mixing in the binary subsystems, a property linked to vacancy energetics and atomic mobility. While not intended for quantitative prediction, it provides qualitative insight into compositional trends in vacancy behaviour and segregation.

Bulk simulations used periodic supercells of $10 \times 10 \times 10$ FCC unit cells (4,000 atoms). We examined Ni–4Al, Ni–8Cr, and Ni–(5, 8, 10, 15)Cr–4Al compositions. Vacancy formation energies E_f were estimated from chemical potentials following Piochaud *et al.* [34], and equilibrium vacancy concentrations c_v were obtained from E_f via Boltzmann statistics. Vacancy migration barriers E_m were computed using the nudged elastic band (NEB) method [35, 36]. Vacancy tracer diffusion coefficients D_{tracer} were calculated from molecular dynamics (MD) simulations at 1300–1400 K with a mono-vacancy in the Isothermal–isobaric (NPT) ensemble . Effective diffusion coefficients were then estimated as $D_{\text{eff}} = c_v\, D_{\text{tracer}}$.

GB segregation was studied using representative coincidence site lattice (CSL) tilt boundaries: $\Sigma3\,(111)$, $\Sigma3\,(112)$, $\Sigma5\,(012)$, $\Sigma5\,(013)$, $\Sigma11\,(113)$, and $\Sigma11\,(332)$. Simulation cells contained 15,000–28,000 atoms depending on orientation and composition. Hybrid Monte Carlo–conjugate gradient simulations were conducted at 1026 K (753 °C) to assess segregation behaviour, and relative enrichment of Al and Cr within 1 nm of the GB was measured.

The Boltzmann-averaged vacancy formation energy for each alloy composition is illustrated in Fig. 1 (black bars). The addition of Cr leads to a systematic **decrease** in formation energy, from 1.60 eV in Ni–4Al to 1.32 eV in Ni–15Cr–4Al.

At equilibrium, the vacancy fraction follows

$$c_v \propto \exp[-E_f/(k_B T)].$$

Thus, a reduction of ∼0.28 eV in E_f (Ni–4Al → Ni–15Cr–4Al) yields vacancy concentrations that are about 11 times higher at 1273 K and more than 54 times higher at 753 K. While absolute vacancy concentrations decrease at lower temperatures, as expected from thermodynamics, the relative enhancement introduced by Cr becomes increasingly pronounced. Cr additions therefore lower vacancy formation energies in the alloy matrix, stabilizing vacancies and amplifying their role in transport processes.

The average vacancy jump barriers are reported in Fig. 1. Green (red, blue) bars represent vacancies exchanging position with Ni (Al, Cr) atoms. Adding Cr to the alloy leads to minimal reduction in barrier height. In other words, Cr addition affects vacancy formation energies, but has almost no effect on migration barriers.

The vacancy tracer diffusion coefficients obtained from MD simulations at 1300, 1350, and 1400 K are shown in Fig. 2(a). Diffusivities increase with temperature. The tracer diffusion coefficients of Ni–4Al, Ni–8Cr, and Ni–8Cr–4Al are broadly similar, indicating that the addition of Cr does

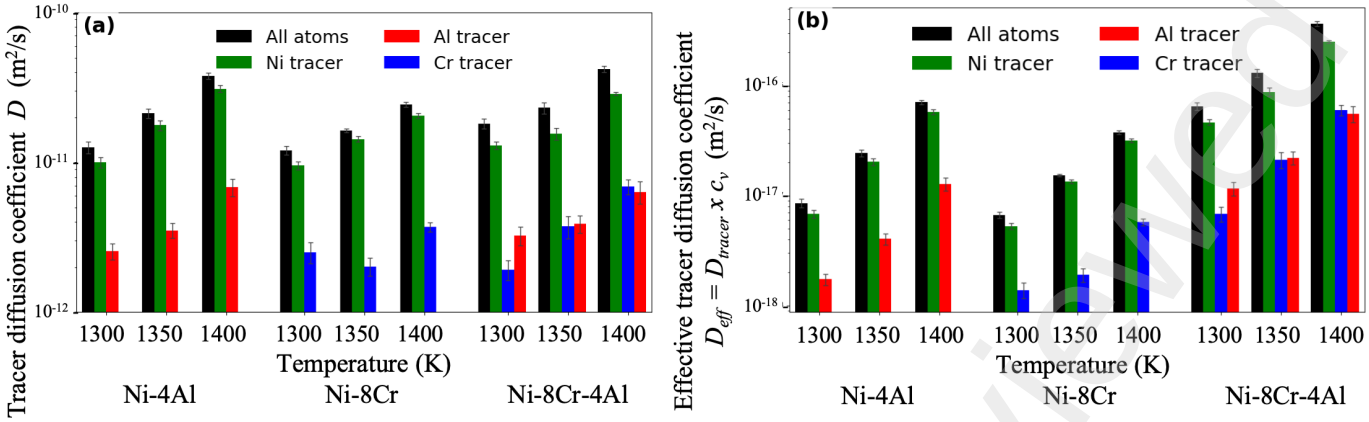

Figure 2: Tracer diffusion in bulk alloys and the effect of equilibrium vacancy concentrations. **(a)**: Tracer diffusion coefficients for a single vacancy in Ni–4Al, Ni–8Cr, and Ni–8Cr–4Al at 1300K, 1350K and 1400K (MD). **(b)**: Effective diffusion coefficients at 1300K, 1350K and 1400K obtained by multiplying tracer values by the corresponding equilibrium vacancy concentrations, revealing an order-of-magnitude increase in the ternary alloy. Error bars represent standard errors.

not strongly alter the overall mobility of individual vacancies, nor their propensity to jump through the Ni, Cr or Al subsystems. This is consistent with the migration barriers presented in Fig. 1: adding Cr has little effect on these barriers.

The simulation results presented in Fig. 2(a) suggest that Al and Cr are intrinsically much more mobile than Ni, despite comprising only 4–8 at.% of the alloys, their tracer contributions nearly match those of Ni to the overall squared displacements. This is also consistent with the migration barriers presented in Fig. 1. The jump barriers involving Al (1.05eV) atoms are lower than those involving Cr (1.1 eV), which are lower than those involving Ni (1.25 eV).

The data presented in Fig. 2(b) includes the effect of equilibrium vacancy concentrations on effective diffusion coefficients. Cr additions have a significant impact on diffusion coefficients. Ni–8Cr–4Al exhibits diffusion coefficients nearly an order magnitude higher than those of Ni–4Al and Ni–8Cr. Cr enhances diffusion primarily by increasing vacancy concentrations, with a muted effect on the mobility of each vacancy.

These calculations help explain high temperature TEE. By lowering vacancy formation energies, Cr substantially increases equilibrium vacancy concentrations, thereby enhancing Al diffusion throughout the alloy. This vacancy-mediated acceleration of Al transport is likely a key contributing factor to the development of continuous Al_2O_3 scales observed experimentally in Ni–Cr–Al alloys[10].

Fig. 4 illustrates typical GB MC–CG simulation results ($\Sigma 5$ (013) shown). In Ni–4Al, Al is uniformly distributed before the MC–CG simulation and segregates to the GB afterward. In Ni–8Cr–4Al, both Al and Cr start uniformly distributed; Al segregates to the GB during the MC–CG run, while Cr does not.

Across all GBs considered, adding Cr to Ni–4Al led to enhanced Al enrichment. On average, relative Al concentration at the GB increased from 121.8% ± 10.6% in Ni–4Al to 151.0% ± 5.7% in Cr-containing alloys, while Cr itself showed little segregation (107% ± 2%) (Fig. 5). Segregation trends varied with GB character, with $\Sigma 5$ and $\Sigma 11$ boundaries generally showing stronger Al enrichment than $\Sigma 3$. $\Sigma 3$ (111) is the twin boundary, and it shows bulk-like behaviour with little segregation towards the grain boundary [9, 10], having a distribution near random as shown in Fig.5. This enhanced Al enrichment at GBs suggests that, even at intermediate temperatures, Cr additions help Ni-Al alloys develop localized Al enrichment along GBs, and the dependence of Al enrichment on GB character is consistent with experimental observation [10].

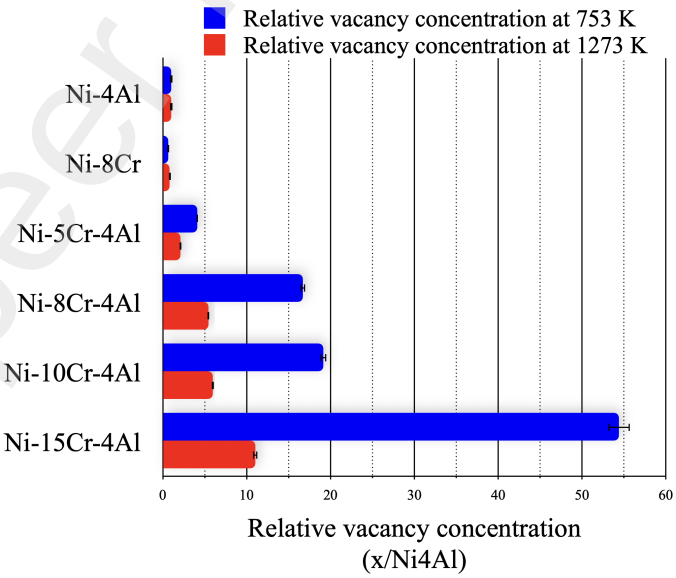

Figure 3: Relative vacancy concentrations in Ni–Cr–Al alloys, normalized to Ni–4Al, at 753 K and 1273 K. Chromium additions markedly increase vacancy concentrations, with the largest effect observed at 753 K.

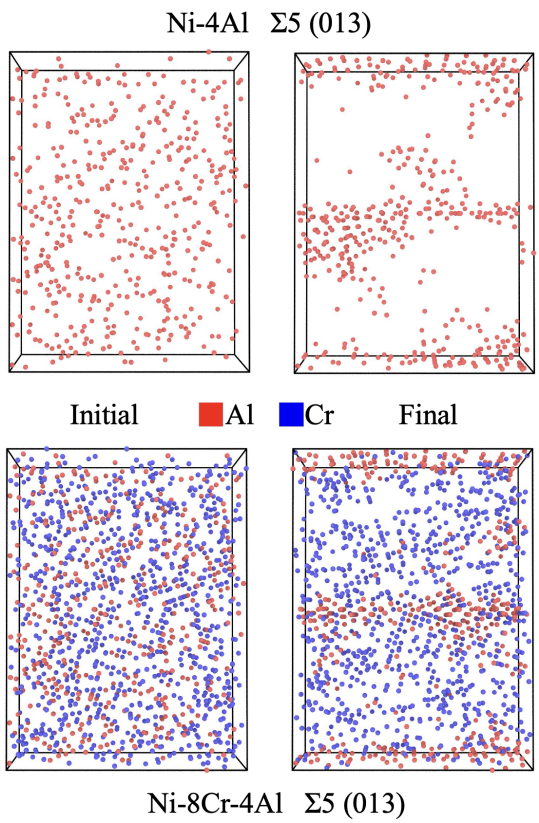

Figure 4: Representative elemental distribution before (left) and after (right) MC–CG simulations. Ni–4Al (top) and Ni–8Cr–4Al (bottom) are shown for a Σ5 (013) GB. Ni is hidden for clarity. Al is the preferred element to segregate at the GB.

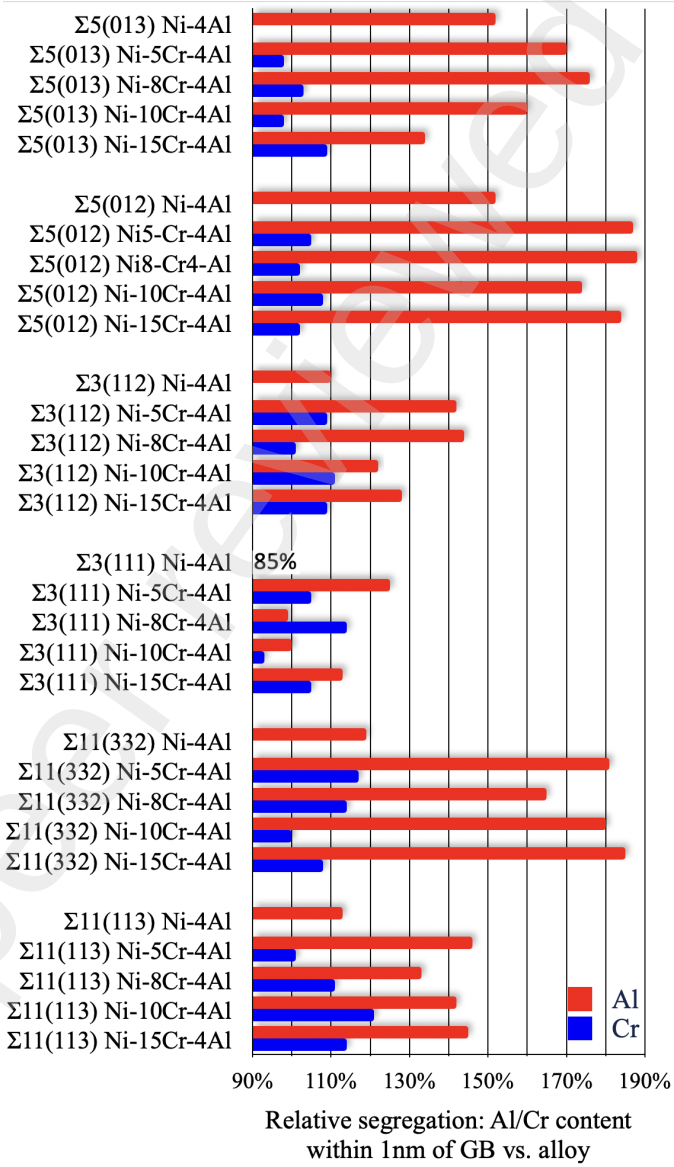

Figure 5: Relative change in concentration of Al and Cr within 1 nm of the GB after MC–CG simulations, normalized to bulk composition. Al segregation is consistently enhanced by Cr additions, while Cr shows little enrichment. Error bars: standard errors across Σ3, Σ5, and Σ11.

Uncertainties reflect bootstrapped means over 1000 random configurations per composition, and GB enrichment error bars denote standard errors across the Σ3, Σ5, and Σ11 boundaries.

Another notable feature is that the concentration profiles of Al and Cr (Fig. 4) resemble the core–shell morphology of intergranular oxides observed experimentally [10], with an Al-rich region at the GB center surrounded by Cr enrichment.

By contrast to the clear relationship between Cr concentration and vacancy formation energy (Fig. 1), we see no systematic increase or decrease in Al segregation once Cr content exceeds Ni–5Cr–4Al (the lowest non-zero Cr content considered herein).

We stress that this vacancy-mediated acceleration of Al transport should be viewed as a *contributing route* to the high temperature TEE, complementing Wagner's oxygen-gettering model.

Several limitations merit discussion. The employment of an EAM potential provides only qualitative trends; more accurate predictions will require density functional theory (DFT) or machine-learned potentials [37–39]. We also did not model atomic diffusion along GBs or explore low-angle and non-CSL boundaries. Finally, the coupling between metallic and oxide phases was not addressed, and only Ni–Cr–Al was considered, whereas the TEE has been observed in many other ternary systems.

The data that support the findings of this study are available from the corresponding author upon reasonable request. The codes that support the findings of this study are available upon request.

This work was supported by the Natural Sciences and Engineering Research Council of Canada (NSERC), Natural Resources Canada (NRCan), and the University Network of Excellence in Nuclear Engineering (UNENE) Research Chair in Corrosion Control and Materials Performance. The authors thank the Digital Resources Alliance of Canada (DRAC), formerly known as Compute Canada, for generous allocation of computer resources.

References

[1] G. Shirane, Y. Yamada, Lattice-dynamical study of the 110 k phase transition in srti o 3, Physical Review 177 (2) (1969) 858.

[2] C. Souza, D. Ribeiro, C. Kiminami, Corrosion resistance of fe-cr-based amorphous alloys: An overview, Journal of non-crystalline solids 442 (2016) 56–66.

[3] N. Sridhar, J. Wu, P. Manning, Corrosion resistant ni-cr-mo alloys, JOM 37 (11) (1985) 51–53.

[4] G. Y. Koga, N. Birbilis, G. Zepon, C. S. Kiminami, W. J. Botta, M. Kaufman, A. Clarke, F. G. Coury, Corrosion resistant and tough multi-principal element cr-co-ni alloys, Journal of Alloys and Compounds 884 (2021) 161107.

[5] Y. Shida, F. Stott, B. Bastow, D. Whittle, G. Wood, Development of preferential intergranular oxides in nickel-aluminum alloys at high temperatures, Oxidation of Metals 18 (1982) 93–113.

[6] P. Scott, M. Le Calver, Some possible mechanisms of intergranular stress corrosion cracking of alloy 600 in pwr primary water, in: Proceedings of the sixth international symposium on environmental degradation of materials in nuclear power systems-water reactors, 1993.

[7] Y. Shi, B. Yang, P. K. Liaw, Corrosion-resistant high-entropy alloys: a review, Metals 7 (2) (2017) 43.

[8] C. Wagner, Passivity and inhibition during the oxidation of metals at elevated temperatures, Corrosion Science 5 (11) (1965) 751–764.

[9] Y. Ghaffari, K. Daub, F. Long, M. Topping, S. Persaud, Comparing the intergranular oxidation of ni-cr and ni-al model alloys in 480° c hydrogenated steam, Scripta Materialia 232 (2023) 115501.

[10] Y. Ghaffari, K. Daub, F. Long, S. Persaud, Intergranular oxidation behaviour of ni-cr-al model alloys in 480 c hydrogenated steam, Corrosion Science 226 (2024) 111678.

[11] R. S. Ullberg, X. Bognárová, M. R. Tonks, S. R. Phillpot, Energetics and diffusion kinetics of point defects in cr2o3 from first-principles, The Journal of Physical Chemistry C (2025).

[12] A. Banerjee, E. F. Holby, A. A. Kohnert, S. Srivastava, M. Asta, B. P. Uberuaga, Thermokinetics of point defects in α-fe2o3, Electronic Structure 5 (2) (2023) 024007.

[13] P. Xiao, C. A. Orme, S. R. Qiu, T. A. Pham, S. Cho, M. Bagge-Hansen, B. C. Wood, Atomic-scale understanding of oxide growth and dissolution kinetics of ni-cr alloys, Nature Communications 16 (1) (2025) 341.

[14] Y. Osetsky, A. V. Barashev, L. K. Béland, Z. Yao, K. Ferasat, Y. Zhang, Tunable chemical complexity to control atomic diffusion in alloys, npj Computational Materials 6 (1) (2020) 38.

[15] K. Ferasat, T. D. Swinburne, P. Saidi, M. R. Daymond, Z. Yao, L. K. Béland, Interstitialcy-based reordering kinetics of ni3al precipitates in irradiated ni-based super alloys, Materialia 19 (2021) 101180.

[16] K. Ferasat, Y. N. Osetsky, A. V. Barashev, Y. Zhang, Z. Yao, L. K. Béland, Accelerated kinetic monte carlo: A case study; vacancy and dumbbell interstitial diffusion traps in concentrated solid solution alloys, The Journal of Chemical Physics 153 (7) (2020).

[17] P. Saidi, P. Changizian, E. Nicholson, H. K. Zhang, Y. Luo, Z. Yao, C. V. Singh, M. R. Daymond, L. K. Béland, Effect of he on the order-disorder transition in ni 3 al under irradiation, Physical Review Letters 124 (7) (2020) 075901.

[18] Y. N. Osetsky, L. K. Béland, R. E. Stoller, Specific features of defect and mass transport in concentrated fcc alloys, Acta Materialia 115 (2016) 364–371.

[19] N. Nepsha, N. Y. Sdobnyakov, V. Samsonov, I. Talyzin, A. Y. Kolosov, D. Zhigunov, K. Savina, A. Romanov, Atomistic simulation of segregation in ternary pt–pd–ni nanoalloy, Journal of Surface Investigation: X-ray, Synchrotron and Neutron Techniques 18 (6) (2024) 1388–1394.

[20] E. Moore, P. Turchi, V. Lordi, D. Weiss, Z. Sims, H. Henderson, M. Kesler, O. Rios, S. McCall, A. Perron, Thermodynamic modeling of the al-ce-cu-mg-si system and its application to aluminum-cerium alloy design, Journal of Phase Equilibria and Diffusion 41 (2020) 764–783.

[21] S. Mahmoud, N. Mousseau, Long-time point defect diffusion in ordered nickel-based binary alloys: How small kinetic differences can lead to completely long-time structural evolution, Materialia 4 (2018) 575–584.

[22] Y. N. Osetsky, L. K. Béland, A. V. Barashev, Y. Zhang, On the existence and origin of sluggish diffusion in chemically disordered concentrated alloys, Current Opinion in Solid State and Materials Science 22 (3) (2018) 65–74.

[23] D. Rohrberg, K.-H. Spitzer, L. Dörrer, A. J. Kulińska, G. Borchardt, A. Fraczkiewicz, T. Markus, M. H. Jacobs, R. Schmid-Fetzer, Host atom diffusion in ternary fe-cr-al alloys, Metallurgical and Materials Transactions A 45 (2014) 269–279.

[24] L. K. Béland, G. D. Samolyuk, R. E. Stoller, Differences in the accumulation of ion-beam damage in ni and nife explained by atomistic simulations, Journal of Alloys and Compounds 662 (2016) 415–420.

[25] C. Reimer, P. Saidi, C. Casert, C. Beeler, C. Tetsassi Feugmo, S. Whitelam, E. Mansouri, A. Martinez, L. Beland, I. Tamblyn, Prediction of vacancy defect diffusion paths in high entropy alloys via machine learning on molecular dynamics data, Journal of Applied Physics 138 (7) (2025).

[26] S. Zhao, Y. Osetsky, Y. Zhang, Preferential diffusion in concentrated solid solution alloys: Nife, nico and nicocr, Acta Materialia 128 (2017) 391–399.

[27] S. Zhao, On the role of heterogeneity in concentrated solid-solution alloys in enhancing their irradiation resistance, Journal of Materials Research 35 (8) (2020) 1103–1112.

[28] B. Xu, M. Jiang, S. Ma, J. Zhang, Y. Xiong, S. Huang, X. Xiang, H. Fu, W. Lu, H. Deng, et al., Revealing the interstitial-mediated sluggish diffusion mechanism in concentrated solid-solution alloys via machine learning-integrated kinetic monte carlo, Physical Review Materials 9 (7) (2025) 073608.

[29] B. Xu, S. Ma, Y. Xiong, J. Zhang, S. Huang, J.-J. Kai, S. Zhao, Exploring the influence of percolation on vacancy-mediated diffusion in cocrni multi-principal element alloys, Materials & Design 223 (2022) 111238.

[30] S. Zhao, Y. Osetsky, Structural and chemical disorder enhance point defect diffusion and atomic transport in ni3al-based γ" phase, Acta Materialia 207 (2021) 116704.

[31] S. Zhao, Y. Osetsky, Y. Zhang, Atomistic simulation of defect-dislocation interactions in concentrated solid-solution alloys, Physical Review Materials 3 (10) (2019) 103602.

[32] A. P. Thompson, H. M. Aktulga, R. Berger, D. S. Bolintineanu, W. M. Brown, P. S. Crozier, P. J. In't Veld, A. Kohlmeyer, S. G. Moore, T. D. Nguyen, et al., Lammps-a flexible simulation tool for particle-based materials modeling at the atomic, meso, and continuum scales, Computer physics communications 271 (2022) 108171.

[33] D. Farkas, A. Caro, Model interatomic potentials for fe–ni–cr–co–al high-entropy alloys, Journal of materials research 35 (22) (2020) 3031–3040.

[34] J. Piochaud, T. Klaver, G. Adjanor, P. Olsson, C. Domain, C. Becquart, First-principles study of point defects in an fcc fe-10ni-20cr model alloy, Physical Review B—Condensed Matter and Materials Physics 89 (2) (2014) 024101.

[35] G. Henkelman, B. P. Uberuaga, H. Jónsson, A climbing image nudged elastic band method for finding saddle points and minimum energy paths, The Journal of chemical physics 113 (22) (2000) 9901–9904.

[36] G. Henkelman, H. Jónsson, Improved tangent estimate in the nudged elastic band method for finding minimum energy paths and saddle points, The Journal of chemical physics 113 (22) (2000) 9978–9985.

[37] V. Deringer, M. Caro, G. Csányi, Machine learning interatomic potentials as emerging tools for materials science, Advanced Materials 31 (2019) 1902765. doi:10.1002/adma.201902765.

[38] Y. Mishin, Machine-learning interatomic potentials for materials science, Acta Materialia 214 (2021) 116980. doi:10.1016/j.actamat.2021.116980.

[39] T. Mueller, A. Hernandez, C. Wang, Machine learning for interatomic potential models, The Journal of Chemical Physics 152 (2020) 050902. doi:10.1063/1.5126336.